GEOMETRICAL DEPENDENCE OF RANDOM LASER ACTION IN ZNO NANOSTRUCTURES GROWN BY CHEMICAL BATH DEPOSITION

NURIZATI BINTI ROSLI

UNIVERSITI SAINS MALAYSIA

2022

GEOMETRICAL DEPENDENCE OF RANDOM LASER ACTION IN ZNO NANOSTRUCTURES GROWN BY CHEMICAL BATH DEPOSITION

by

NURIZATI BINTI ROSLI

Thesis submitted in fulfillment of the requirements
for the degree of
Doctor of Philosophy

October 2022

ACKNOWLEDGEMENT

In the name of Allah, the Most Gracious, the Most Merciful.

All praise be to Allah, without His Graciousness and Mercy, this thesis would not come into existence. This thesis is dedicated to my lovely family, my dad Rosli Abu Bakar, mom Siti Fazlina Abdullah, siblings, Muhamad Syafiq, Nur Ayuni, Nur Atikah, Muhammad Syamil, and Muhammad Syahir, also family in law. To my dad, mom, husband Muhammad Farid and dear son Muhammad Thaqif, thanks for all support, advice, love, patience, care, concern and helping me to finish this study. This journey from the beginning till the end of my Doctor of Philosophy would not be possible without them.

I am extremely grateful for the assistance and guidance of my supervisor, Dr Mohd Mahadi Halim. Without his continuous support, guidance, and knowledge in many matters, this thesis would not have seen the light of day. My gratitude and thank also goes to my co-supervisor, Prof. Dr Md Roslan Hashim and Dr Wan Maryam Wan Ahmad Kamil, for their gentle but firm guidance and support, besides being always open to me whenever I need assistance and help to improve myself throughout this journey. To the staffs at INOR and NOR Lab, mainly Pn Ee Bee Choo, En Abdul Jamil Yusuf, En Yushamdan Yusof, Pn Mahfuzah Mohd Fuad, Pn Aznorhaida Ramli, En Mohtar Sabdin, and others, I thank you for your technical assistance and guidance throughout my journey here. I am also grateful for the RUI grant under School of Physics, Universiti Sains Malaysia 1001/PFIZIK/8011092 in supporting all the experimental materials and expenses. Last but not least, I thank all of my friends, Syairah, Hidayah, Syahida, Atieqah, Mimi, Zira, Ainita, Zulfa, Puteri, Abdullah, Suvind, Kevin, and Ahlaam.

To everyone and everything, thank you.

TABLE OF CONTENTS

LIST OF FIGURES

Page

LIST OF TABLES

Page

LIST OF APPENDICES

$A/s/cm^2/K$	Pyroelectric constant
a_o	Lattice parameter of *a*
β	Beta factor of laser
c	Speed of light in vacuum
cm	Centimeter
c_o	Lattice parameter of *c*
$\cos\theta$	Average cosine of the scattering angle
$D(\lambda)$	Diffusion constant of light
dt	Probability in time
E	Electric field
E_a	Lower energy level
E_b	Higher energy level
eV	Electronvolt
$\varepsilon(x)$	Microscopic permittivity
g/cm^3	Gram per cubic centimetre
g/mol	Grams per mole
h	Planck's constant
H	Magnetic field
$JK^{-1}mol^{-1}$	Joules per kelvin per mole
k	Boltzmann's constant
k	Bloch wavenumber
kcal/mole	Kilocalorie per mole

kJ/mol	Kilojoules per mole
L	Medium thickness, sample size
ℓ_s	Scattering mean free path
ℓ_t	Transport mean free path
M	Molarity
m_e	Electron effective mass
meV	Milli electron volt
mg	Milligram
mg/L	Milligrams per liter
m_h	Hole effective mass
n	Index of refraction
nD	Refractive index standards
$\hat{n}$	Vector normal to the boundary
$N_1(t)$	Number of excited molecules
$P(t)$	Pump rate
$q(t)$	Number of photons in laser modes
T	Temperature
τ	Spontaneous emission lifetime
τ_c	Cavity decay time
$u(x)$	Eigenvalue of function
v	Speed of light in medium, frequency
ε_∞	Dielectric constant
λ_{light}	Wavelength of light

ρ	Number density of scattering particles
$\rho(v,T)$	Spectral density
σ_s	Cross-section of the scattering particles
$\mu(x)$	Permittivity of the photonics/metamaterials crystal
%	Percentage
°C	Degree celsius
1D	One dimensional
2D	Two dimensional
3D	Three dimensional
CBD	Chemical bath deposition
CdO	Cadmium oxide
CdS	Cadmium sulfide
CdSe	Cadmium selenide
CH_2O	Formaldehyde
CR	Carbothermal reduction
$CuInS_2$	Copper indium sulfide
$CuInSe_2$	Copper indium selenide
CVD	Chemical vapor deposition
cw PL	Continuous-wave photoluminescence
DI	Deionization
EDX	Energy-dispersive X-ray
EM	Electromagnetic
FESEM	Field Emission Scanning Electron Microscope

HMTA	Hexamethylenetetramine
ITO	Indium tin oxide
LA	Laser ablation
MBE	Molecular beam epitaxy
NCFlowers	Nanocauliflowes
NFlakes	Nanoflakes
NH_3	Ammonia
NRods	Nanorods
NSDers	Nanospiders
NSs	Nanostructures
NWalls	Nanowalls
PbS	Lead (II) sulfide
pC/N	Picocoulomb per newton
pw μ-PL	Pulsed-wave micro-photoluminescence
RL	Random laser
SnS_2	Tin (IV) sulfide
TiO_2	Titanium dioxide
UV	Ultraviolet
UV-Vis	Ultraviolet-Visible
XRD	X-Ray Diffraction
$Zn(NO_3)_2.6H_2O$	Zinc nitrate hexahydrate
ZnO	Zinc Oxide

KEBERGANTUNGAN GEOMETRI KE ATAS TINDAKAN LASER RAWAK DALAM NANOSTRUKTUR ZNO DITUMBUHKAN OLEH PEMENDAPAN RENDAMAN KIMIA

ABSTRAK

Zink oksida (ZnO) telah menarik minat komuniti penyelidikan kerana mempunyai ciri optik dan struktur yang istimewa seperti jurang jalur terus yang lebar pada 3.37 eV, dan tenaga pengikatan eksiton pada 60 meV. Justeru itu, banyak kajian yang membentangkan pelbagai teknik pertumbuhan untuk sintesis nanostruktur (NSs) ZnO melalui proses fabrikasi yang kompleks seperti proses sol-gel dan kaedah koloid [1,2], sintesis gas berfasa (kaedah semburan pirolisis dan pemeluapan gas lengai) [3] dan banyak lagi. Dalam kajian ini, pelbagai nanostruktur (NSs) ZnO dihasilkan melalui pemendapan rendapan kimia (CBD) menerusi pengumpalan heksametil tetramin (HMTA) dan zink nitrat heksahidrat ($Zn(NO_3)_2.6H_2O$), pada suhu 96 ^oC selama 3 jam. Sebelum proses penumbuhan berlaku, lapisan benih dipercikkan bagi mengurangkan tenaga lapisan serta menyediakan tapak penukleusan untuk NSs. Pengubahan parameter CBD seperti kepekatan molariti, keasidan dan kealkalian (keadaan pH) pada larutan pelopor akan mempengaruhi pertumbuhan NSs. Sifat struktur dan sifat optik ZnO NSs dikaji oleh mikroskop pengimbas pancaran medan elektron (FESEM), penyebaran tenaga sinar-X (EDX), spektrum belauan sinar-X (XRD), cahaya ultraungu kelihatan (UV-Vis), dan pengukuran gelombang selanjar fotopendarkilau (cw PL). Dengan mengawal parameter bagi kaedah CBD, ciri unik geometri boleh diperhatikan oleh FESEM seperti NSs berorientasikan rawak, nanorod, nanodinding, nanokepingan heksagon jelas,

nanobungakubis, dan nanosawang. Analisis XRD menunjukkan fasa spektrum belauan yang serupa pada (002), analisis UV-Vis membuktikan jurang jalur dalam julat UV (antara 3.18 eV hingga 3.29 eV) untuk semua parameter, sementara cw-PL menunjukkan sedikit berhampiran pinggir jalur (NBE) puncak berbanding dengan nilai yang terdapat dalam ZnO sebenar. Semua ini membuktikan bahawa NSs tersebut memiliki sifat yang sama dalam banyak aspek dari struktur pukal. Ciri-ciri ini membuka banyak peluang dalam aplikasi dan salah satunya adalah untuk menghasilkan laser rawak (RL) ambang rendah pada suhu bilik. Hasil dari pelbagai geometri ZnO NSs ini diuji untuk memerhatikan tingkah laku RL dengan analisis pungukuran gelombang denyut mikro fotopendarkilau (pw μ-PL). Hasil kajian menunjukkan bahawa pancaran ambang dan panjang gelombang dapat disesuaikan dengan parameter pertumbuhan yang berbeza-beza ketika proses CBD. Peningkatan kepekatan molariti CBD, ambang RL telah menurun (dari 294.37 kW/cm^2 ke 14.29 kW/cm^2) ke arah molariti CBD yang besar dan juga mencapai zarah terbesar dengan penghabluran tertinggi NSs. Tingkah laku RL menunjukkan kecenderungan yang serupa terhadap penukaran keadaan pH. Terdapat pelbagai model, yang kebanyakannya model percubaan matematik untuk menggambarkan tindakan RL secara umum [4,5]. Oleh itu, kajian ini adalah untuk membentuk model yang mudah menggunakan simulasi unsur terhingga dilakukan menggunakan COMSOL Multiphysics. Hal ini untuk menjelaskan laluan serakan rawak yang menunjukkan kepada tindakan laser rawak dalam struktur pada panjang gelombang ambang rendah yang dipilih. Secara keseluruhannya, laser yang stabil serta bilangan mod yang terhad, dan pancaran RL ambang rendah dicapai dengan keterujaan ketumpatan daya cahaya dalam julat kW/cm^2 hingga MW/cm^2. Geometri ZnO NSs yang tersendiri menawarkan potensi yang sangat baik untuk mencapai pancaran RL dan ini dapat membuka peluang yang lebih luas bagi aplikasi dan sistem nanofotonik.

GEOMETRICAL DEPENDENCE OF RANDOM LASER ACTION IN ZNO NANOSTRUCTURES GROWN BY CHEMICAL BATH DEPOSITION

ABSTRACT

Zinc oxide (ZnO) has attracted considerable interest in the research community for its distinctive optical and structural characteristics such as wide direct band gap at 3.37 eV, and large exciton binding energy at 60 meV. Thus, numerous work presented various growth techniques to synthesize ZnO nanostructures (NSs) through a complex fabrication process such as sol-gel process and colloidal method [1,2], gas phase synthesis (spray pyrolysis and inert gas condensation methods) [3] and more. In this work, various ZnO NSs were prepared by simple deposition technique known as chemical bath deposition (CBD) through the agglomeration of the hexamethylenetetramine (HMTA) and zinc nitrate hexahydrate ($Zn(NO_3)_2.6H_2O$), at an elevated temperature of 96 ^oC for 3 hours. Prior to the growth process, a seed layer was deposited to reduce the interface energy and provide the nucleation site for the NSs. Varying CBD parameters such as molarity concentration, acidity, or basicity (pH conditions) of the precursor solution affect the growth of the NSs. The structural and optical properties of ZnO NSs were investigated by Field Emission Scanning Electron Microscope (FESEM), energy-dispersive X-ray (EDX), X-Ray Diffraction (XRD), UV-Visible (UV-Vis) analyses, and continuous-wave photoluminescence (cw PL). By controlling the CBD parameters, unique geometrical features were observed by FESEM such as randomly oriented NSs, nanorods (NRods), nanowalls (NWalls), sharp hexagonal nanoflakes (NFlakes), nanocauliflowers (NCFs), and nanospiders (NSDers). The XRD analysis revealed similar preferential (002)

diffraction phase, UV-Vis analysis proved the band gap within the UV range (between 3.18 eV to 3.29 eV) for all variations, while cw PL show a slightly shifted of near-band-edge (NBE) peaks as compared to the values found in bulk ZnO. All these results proved that the structures owned identical properties in many aspects to their bulk counterpart. These features open all sorts of possibilities in application and one of it is for making low-threshold random laser (RL) at room temperature. The performance of these variety of ZnO NSs were further tested to observe the RL behavior by pulsed-wave micro-photoluminescence (pw μ-PL) analysis. The results revealed that the emission threshold and wavelength were tunable by varying growth parameters during the CBD process. By increasing of CBD equimolar concentration, RL threshold were reduced (from 294.37 kW/cm^2 to 14.29 kW/cm^2) toward highest CBD molarity which also achieved the biggest particle and the highest crystallinity of the NSs. RL behavior showed a similar trend toward varying on pH conditions. There were various models, mostly mathematical attempted to describe the RL action in general [4,5]. Thus, this work construct a simple model using finite element simulation was carried out using COMSOL Multiphysics. This elucidate the random scattering path that leads to random lasing action in the structure at the chosen emission wavelength. Overall, a stable, limited number of lasing modes, and low threshold RL emission were achieved by excitation power density in a range of kW/cm^2 to MW/cm^2. The distinctive ZnO NSs geometry offers excellent potential to achieve RL emission and this could open wider opportunities to be utilized in the nanophotonic systems and applications.

CHAPTER 1: INTRODUCTION

1.1 Introduction

This chapter will clarify the background, problem statement, research objectives, scope of study, and thesis organization of this work entitled “Geometrical Dependence of Random Laser Action in ZnO Nanostructures Growth by Chemical Bath Deposition”.

1.2 Background

Zinc Oxide (ZnO) has attracted a lot of research interest from many researchers worldwide over the past decade, especially as semiconductor devices due to its unique structure, optical, and electronic properties. ZnO is II-VI compound semiconductor with a band gap of 3.37 eV and a large exciton binding energy of 60 meV for excitonic transitions even at room temperature, high radiative recombination efficiency for spontaneous emission and is highly transparent in the visible spectrum [6]. The applications of ZnO are not limited only to the opto/electro/photonics applications but also in the coating, cosmetic, medical, and food packaging industries [7–10]. In the photonics field, ZnO is commonly used as the active medium [11,12]. This semiconductor material operates well as a scattering medium, emit UV light via optical pumping, and eliminated the energy-efficient device's undesirable deficiencies [13]. ZnO is also well known to intrinsically behave as an n-type semiconductor and naturally crystallizes in

wurtzite structure [14]. In addition, ZnO can be formed in many geometrical shapes of NSs, which can be obtained by using different synthesis methods. ZnO is easy to fabricate with uniform growth using a top-down or bottom-up approach, abundant, and environmentally friendly [15,16]. The growth of ZnO NSs can be realised through numerous techniques such as chemical processes at high temperatures, complicated and cost demand-which is known as molecular beam epitaxy (MBE), chemical vapor deposition (CVD), carbothermal reduction (CR), and laser ablation (LA) [17]. Aside from that, simple solution methods can also be part of the options, such as chemical precipitation, sol-gel synthesis, chemical bath deposition (CBD), and hydrothermal reaction [18,19]. CBD is considered as one of the most straightforward methods, cheaper, facile, low-temperature bath process, a simple self-engineered experimental work that provided a large growth surface area, synthesized NSs were uniform, high quality, and good adherent of NSs can be obtained [20,21]. Furthermore, through CBD, controllable compound deposition and tunable morphology can be achieved by controlling certain growth parameter, that yields stable and uniform nanostructure growth, for a promising photonic device performance [22].

Intrinsically, ZnO possess a natural scattering action for optical gain that leads to localization of light throughout its medium which could results in random lasing (RL) emission [23]. In these days, different types of lasers have been developed beyond the traditionally known concept and design. Random laser was known as one of the non-conventional lasers. This device amplifies light in the gain medium to produce intense monochromatic light [24,25]. The RL has a feedback mechanism that was built upon disorder-induced multiple scattering within the material [26]. Fundamentally, RL design and operation is very interesting to study due to its simplicity, stability, and wide

excitation area, as well as the fact that it provides several possibilities for controlling the photon transport behaviors. In the presence of strong scattering and gain, repeated closed-loop path could provide coherent feedback and resulting in lasing action [27,28]. Numerous works were carried out to modify with the intension to achieve a much lower threshold, but this was difficult due to the limitations of the chosen materials. There are several factors that influenced the lasing threshold and these include the type of material [29], lattice shape [30], size and shape of the scattering media [31], packing density of scatterer resonant/dense medium [32], sample thicknesses [33], and more. It had been proposed that RL emission arises due to propagation of light that was hindered in strong scattering media and forming a closed loop. The light was said to become localized, which analogous to Anderson localization of electron in amorphous material. When substantial optical gain reaching a certain threshold, and combined with the multiple scattering process that occurs throughout the medium, the emission output was known as random laser [32,33].

1.3 Problem Statement

There are two major problem statements outlined in this research, listed as follows;

a) Much effort dedicated so far reveals the observation of RL action in various forms of ZnO structures by various methods that involve with high temperatures, complicated and cost demanding [34–38]. However, no work was done regarding the study of structural dependence properties only by tuning CBD growth parameters. The RL effect so far was

understood to occur when propagation of light is hindered by the scattering material inside the gain medium which leads to amplification and stimulation of light out of the structure. However, RL action from ZnO nanostructures occur within the same material, playing both the role of the gain medium as well as scattering material. The outcome from this work will reveal the role of material geometry of ZnO NSs in scattering and amplifying light as RL. By finding the geometrical dependence relation growth by simple CBD method, conclusive evidence would help to elucidate further this interesting phenomenon.

b) Numerous models, mostly mathematically, existed to explain the process that leads to the RL action in general [25,39,40]. But no conclusive model existed to explain the role of structural geometry. Thus, a graphical model that could simulate this by COMSOL Multiphysics would be a proper advantage.

1.4 Research Objectives

The focus of this work were on synthesis, characterization, and studies on the geometrical dependence of RL action in ZnO NSs grown by CBD. There are few variations of CBD parameters that will affect the growth of the NSs, such as concentration molarity, and addition of acid and alkali by tuning the pH conditions of CBD solution. To achieve this, the following objectives have been proposed to guide the research direction. The research objectives are outlined as follows:

a) To synthesize and characterize the physical, structural, and optical properties of the ZnO NSs with various geometry by CBD.

b) To investigate the dependence of random lasing action in various ZnO NSs.

c) To validate the random lasing with COMSOL Multiphysics.

1.5 Scope of Study

Based on the objectives, the scope of the study was planned as follows;

(a) Synthesis of ZnO NSs by several variation in parameters of equimolar concentration (0.01 M to 0.25 M) and adding small molarities of acid ($C_6H_8O_7$), and alkali (NH_4OH) into the bath solution.

(b) The characterization and observation works were carried out through FESEM, XRD, UV-Vis, and cw PL.

(c) RL observation and measurements were done by a pw μ-PL system.

(d) Simulation models of EM waves path propagation with strong EM confinement were develop using COMSOL Multiphysics software to correlate the models with the experimental observations on RL emission.

1.6 Thesis Outline

This thesis contains five chapters in which a comprehensive study on geometrical dependence of RL action in ZnO NSs grown by CBD is presented. The thesis organization is prepared by chapter, based on the following;

Chapter 1 presents an introduction, problem statement, research objectives, the scope of the study, and thesis organization of this thesis.

Chapter 2 provides literature reviews such as theories, basic properties, growth mechanism, structural properties, and optical properties from books, papers, and journals on ZnO NSs and RL emission.

Chapter 3 provides details of basic/working principle, fundamentals, equipment used for and sample preparation by different characterization methods of FESEM, EDX, XRD, UV-Vis spectroscopy, cw PL setup, and pw μ-PL setup.

Chapter 4 focuses on data analysis, explanations of the data, and analysis of results obtained from the listed characterization tools and equipment.

Chapter 5 presents the conclusions of this work and suggestions for the future work. The conclusion will summarize all the results. Future work will give several new notions for the next studies.

CHAPTER 2: LITERATURE REVIEW

2.1 Concept of Light Propagation

Light propagation is commonly understood as the transfer of electromagnetic wave from one point to another. Light travels at the speed of 2.98 x 10^8 m/s in vacuum and the propagation can take place through various mediums including solid, liquid, gas, as well as a state of random molecules arrangement. The speed of light that travels in a given medium can be related to the index of refraction *n*, which is provided by Equation 2.1,

$$n = \frac{c}{v} \tag{2.1}$$

where *c* is the speed of light in vacuum and *v* is the speed of light in the medium. The speed of light in any medium would be lower than in a vacuum (< 2.95 x 10^8 m/s). The propagation of light is concerned with absorption, re-emission, and scattering of the wave by the atom of the medium. The light scattering in the medium is keen on repeatedly in different directions (in gaseous/random arrangement), thus producing light in the UV or visible spectrum. The effective speed at which an electromagnetic wave passes through a medium is determined by two primary factors: the magnitude of the delay (absorption and re-emission process) and how packed is the atom arrangement. Mainly, the scattering effect governs the interaction of electromagnetic radiation with photonic materials (e.g. ZnO) as the refractive index (around 2) [41] is larger than base material (e.g. glass) which approximately (1 to 1.5) [42–44]. Scattering is the process of light interacts with photonic

materials, and having a high refractive index difference between the scattering particles and the background material ensures substantial scattering, as in Figure 2.1 [45],

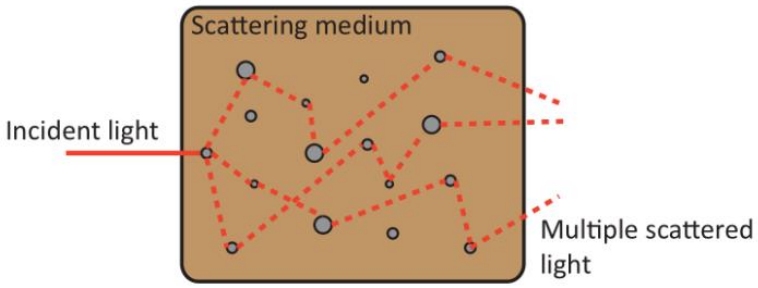

Figure 2.1: Photons trajectories in a high scattering medium [45].

Photons could be scattered numerous times when travelling through a medium, based on the relative thickness of the medium compared with its scattering mean free path, ℓ_s. ℓ_s is specified as the average distance travelled by light over two consecutive scattering events as in Equation 2.2,

$$\ell_s = \frac{1}{\rho\sigma_s} \tag{2.2}$$

where ρ is the number density and σ_s is the cross-section of the scattering particles. Figure 2.2 shows three regimes that can be specified for different propagating in disordered media [46].

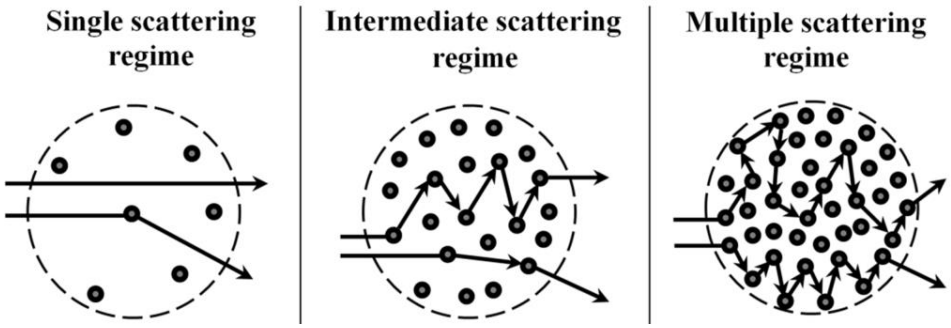

Figure 2.2: Classification of scattering media from optically dilute to intermediate to dense media [46].

Equation 2.3 presents the ballistic regime (dilute) in which the photons are practically not scattered and only by absorption action occur. Photon is transmitted in the same direction as the incoming beam [47].

$$L \ll \ell_s \tag{2.3}$$

where L is the medium thickness and ℓ_s is the scattering mean free path. Equation 2.4 presents the diffused scattering regime (thin sample), which plays both roles between the ballistic and multiple scattering, as the thickness is approximately the same as the mean free path.

$$L = \ell_s \tag{2.4}$$

Equation 2.5 denotes the multiple scattering regime. The multiple scattering regime is the transport of electromagnetic energy only through diffused light, and a random walk model can describe the diffuse action of photon propagation [48].

$$L \gg \ell_s \tag{2.5}$$

2.2 Absorption, Spontaneous, and Stimulated Emission

Several different phenomena occur during photon absorption inside an optical substrate. Electrons absorb radiative photons at discrete energy levels of the optical medium, and excited to the higher energy levels. Einstein proposed the probability in time of the transition of atom in the lower energy by absorbing the illuminated photon from energy level *a* to *b* based on the quantum state as in Equation 2.6,

$$dW = \rho(v,T)\, B_{ab}\, dt \tag{2.6}$$

where $\rho(v,T)$ is spectral density, v is frequency, T is temperature, and B_{ab} is a constant. Equation 2.7 exploits the action when electrons fall to a lower energy state or termed de-excitation (spontaneous photon emission). These molecules fluoresce and emit radiation (photons) by spontaneous emission. Einstein proposed the probability in time, *dt*,

$$dW = A_{ba}\, dt \tag{2.7}$$

where A_{ba} is constant from lower energy level, *a* to a higher energy level, *b*. The total energy of the photon produced by an atom when spontaneous emission occurs is proportional to the energy difference between the excited state and lower energy states. The emitted photon is isotropic and radiates in all directions (fluorescence) caused by impurities in the sample substrate.

In a conventional laser system, stimulated emission and photon scattering lead to reduction in efficiency. However, in a disordered medium system, multiple scattering can lead to the increase in both oscillations and amplifications. Light amplification can be achieved using a scattered gain medium that correlates multiple photon scattering and offers feedback within the active medium [49]. In 1917, Einstein debated that a radiation field triggered electrons in the higher energy state to transition to the lower energy state

known as stimulated emission. He then proposed the stimulated emission mechanism that could lead to amplification of light. Einstein further postulated the probability of transition in time, *dt* as in Equation 2.8 [50],

$$dW = \rho B_{ba}\, dt \tag{2.8}$$

where B_{ba} is constant from higher energy level, *b* to lower energy level, *a*. The process of transition between the energy state emits monochromatic radiation at Bohr's frequency condition from state *b* to *a* as in Equation 2.9 [50],

$$v = (E_b - E_a)/h \tag{2.9}$$

where E_b is the higher energy level, E_a is the lower energy level, and *h* is Planck's constant. Thus, Einstein executed Planck's constant radiation law for the atom in achieving the thermal equilibrium in Equation 2.10 [50],

$$v = (8\pi h v^3/c^3)/(\exp(hv/k\mathrm{T})) \tag{2.10}$$

where *k* is Boltzmann's constant and *T* is temperature in Kelvin.

2.3 Random Laser

In conventional laser systems, a gain medium and reflector or partial reflector (mirror) offer coherent, positive feedback to the gain medium, as shown in Figure 2.3(a). As for RL, reflectors were not required and instead the intense multiple scattering built up in a disordered gain medium as in Figure 2.3(b). RL refers to light amplification by stimulated emission of electromagnetic radiation within a randomly oriented and highly scattering medium [51]. Within the active medium of RL, light is scattered in multiple directions provided that the material's refractive index has a spatial profile. The scattered wave

becomes strongly confined to a small area (similar to a standing wave); that such a photon's mean free path is shorter than its wavelength. This is known as 'Anderson localization'- which originally related to the localization of the electron in disordered solids that may limit metallic conduction in the field of solid state physics [52,53].

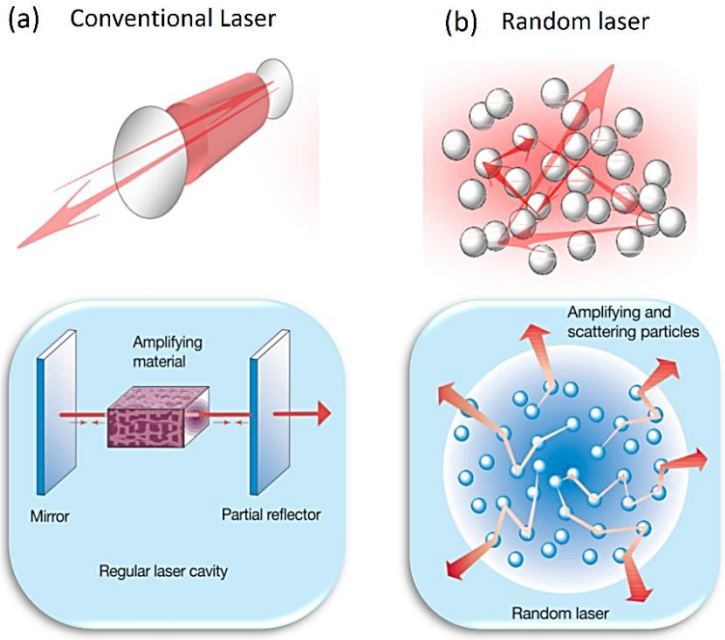

Figure 2.3: Differences between (a) conventional laser with a closed mirror to form amplify laser cavity (Fabry Perot), and (b) RL with randomly oriented scattering particles that can achieve light amplification (random lasing) [51].

RL can be grouped into two main types [54,55]. The first is a single active material that serves as both gain and scattering medium, such as ZnO semiconductor powder which induced the stimulated emission until the lasing threshold is reached. The second type consisted of two different materials that independently act as gain and the other as a

scattering medium, such as laser dye based on a colloidal system. In this case, the laser dye is the gain medium, while the nanoparticles act as the scatterer [56,57].

2.3.1 Theory of Random laser

Lasing emission amplified by a strong scattering within the medium was first proposed in 1966, replacing one of the laser mirror with a scattering medium [58]. Later, Letokhov introduced the scattering region of random walk in RL systems by exploiting and modifying the diffusion equation for the first time in 1968 [59]. Nevertheless, it was thought that scattering in random systems is undesirable for the lasing process because it decreases the coherent feedback of light in conventional laser systems. In 1986, a strong scattering effect was demonstrated on neodymium powders and raises the drastic growth of intensity peaks on high pumping power [60]. In 1994, Lawandy reported the narrowing of spontaneous emission spectrum peaks and multimode of RL peaks, described laser-like emission, and reminded Letokhov's work earlier [61]. This prompted many experimental researchers and theorists to explore the properties of RL further. In 1995, a theoretical work based on the integral method proposed a strong and intense coherent backscattering can be achieved and was introduced later in the RL coherent backscattering (localization) system [62]. In 1996 and 1997, another theoretical model was proposed, merging electron population with diffusion equation and random walk model which lead to a spectra narrowing profile [63,64]. By late 1999 and early 2000, most of the works focused on the theoretical investigation by simulation of RL based on time-independent transfer matrix,

time-independent invariant embedding, also finite-difference time-domain that demonstrate time-dependent and independent focused on RL theories [65–67].

2.3.2 Random Laser Operation

Discussion on RL is interrelated within condensed matter physics based upon the localization of electromagnetic waves in random media and laser physics on the amplification action. Even though the mechanism in RL is different from the conventional laser, the rate of diffusion, photon relaxation behaviors, photon oscillation are very much similar; thus, similar rate equations can be used to model the lasing process in a RL as in Equation 2.11 and 2.12 [68],

$$\frac{N_1(t)}{dt} = P(\mathrm{t}) - \frac{\beta q(t) N_1 t}{\tau} - \frac{N_1(t)}{\tau} \tag{2.11}$$

$$\frac{dq(t)}{dt} = \frac{\beta N_1 t}{\tau}\,(q(t) + 1) - \frac{q(t)}{\tau_{\mathrm{c}}} \tag{2.12}$$

where $N_1(t)$ is the number of excited molecules, $P(t)$ is the pump rate, $q(t)$ is the number of photons in laser modes, β is known as the beta factor of laser, indicated the efficiency of the spontaneous emission toward stimulated emission, τ is the spontaneous emission lifetime, and a laser that involves the average numbers of lasing, τ_c is the cavity decay time that depends on $D(\lambda)$ as in Equation 2.13,

$$\tau_{\mathrm{c}} = \frac{L_2}{8D(\lambda)} \tag{2.13}$$

where L is the sample size and $D(\lambda)$ is the diffusion constant of light. It is conscious that modifying $D(\lambda)$ and/or L can influence the lasing threshold and laser process.

The increase in stimulated emission is attributed to a reduction in spontaneous emission, which means that enhanced stimulated emission associated with inhibited spontaneous emission is achieved. In random media, the mean free path for photons were reduced in a large number of scatterer, which lead to most photons subjected to multiple scattering and amplifications. As a result of the increased residence time of photons within the medium, photon feedback improved while reducing the spontaneous emission background [49].

2.3.3 Scattering Properties of Random Nanostructures

Light scattering occurs when the light is required to change its heterogeneity propagation in a medium. In elastic scattering where the energy of the incident photon is not dissipated (no loss), the photon is scattered in different directions without the changing in wavelength. In random media, the heterogeneity path was commonly created within the nanoparticle that can provide the feedback mechanism. An elastic scattering may be categorized according to the size of the scatterer particles. When the size of the particles is substantially small compared to the wavelength of light, the process is referred to as Rayleigh scattering [69,70]. When the size is bigger, Mie scattering is a more precise model that explains nanoparticle scattering properties, almost the same size as the wavelength of light [71].

To achieve lasing conditions, random lasers should always be operated in similar scenarios as conventional lasers, which are stimulated emission and light trapping (for RL, light trapping is considered as a multiple scattering action process) as in Figure 2.4. The scattering process must be described by employing both of the scattering mean path and the transport mean free path. The average distance a molecule travels between collisions is known as scattering mean path (ℓ_s), the average distance a wave travels before its direction of propagation is randomized is known as the transport mean path (ℓ_t) as given in Equation 2.14,

$$\ell_t = \frac{\ell_s}{1 - \cos\theta} \tag{2.14}$$

where $\cos\theta$ is the average cosine of the scattering angle, and for Rayleigh scattering, $\ell_t = \ell_s$.

The requirements to achieve lasing amplification in random media is optical gain. Multiple scattering effects include system size (L), transport mean free path (ℓ_t), and wavelength of light, (λ_{light}) which depend on two groups of (1) Anderson localized RLs acknowledged as strong interference closed paths, ($\ell_t \leq \lambda_{light}$), and (2) delocalized RLs accredited as weak scattering ($\lambda_{light} < \ell_t < L$). For Anderson localized RLs, it is possible to achieve spatially localized modes and lasing peaks with a line-widths range of 0.01 nm to 0.1 nm. To achieve the random lasing, the threshold behavior must be considered. The indication of a threshold pump intensity is the experimental proof of RL action. A significant kink in the linear plot of a light emission brightness that develops linearly with pump power is generally known as a fluorescence characteristic dominated by stimulated emission.

In RL, a significance coherence feedback allowed for a discrete or only a few modes possibly occurs as Anderson localization system. This coherent feedback avoided the diffusive feedback that owed no sharp lasing peak where it completely disregarded the coherence mode and ignored the closed path. It was recommended that if the system size is smaller than that of the gain length or critical volume, no photon emission can occur, and if the gain becomes too low or the path length is too short, a specific linewidth cannot be assigned to lasing, which refers to as a weaker scattering regime ($\ell_t \geq L$) [72].

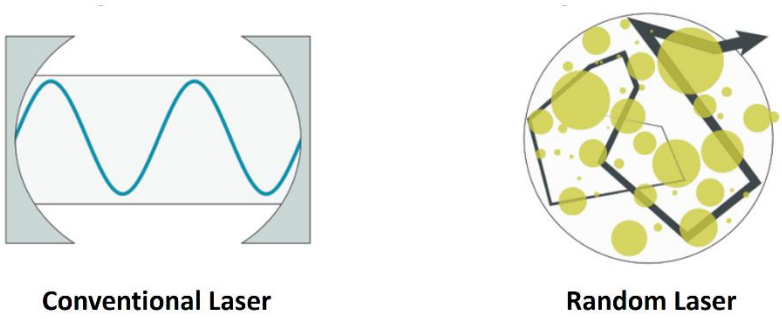

Figure 2.4: Details exploit of conventional laser whereby the lasing was achieved through light trapping within Fabry-Perot cavity (left), and random lasing achieved through multiple scattering in highly disordered medium (right) [72].

2.3.4 Random Laser with Incoherent and Coherent Feedbacks

Non-resonant (incoherent)/feedback lasers were developed for the first time in the late 1960s [59], [73]. Photons are randomly emitted before leaving the gain media and experience repeated scattering by stimulated emission. On the other hand, scattering only

returns a portion of the photons to the gain media, not even to their original position; hence, spatial resonance is absent. The dwell period of light is unaffected by frequency [74]. The scattering direction is changed, and after one loop, it does not return to its previous position. The mean frequency of a random laser is determined solely by the centre frequency of the gain media's emission band.

Meanwhile, for coherent feedback, scattering can produce coherent feedback when scattered light is held to form a closed loop in random media. The interference phenomena in the closed-loop promote the unique characteristic of laser spikes in the spectral emission. The recurrence modes in the system cause these spikes, with very narrow spectral patterns. This led to a significant difference between the properties of a random laser with coherent feedback and those of a random laser with incoherent feedback, as in Figure 2.5. Besides, the recurring scatterings in both strong and weak scattering regimes can offer coherent feedback. A strong scattering refers to the Ioffe-Regel criterion where the multiple interferences continue to dominate all through scattering that effects suppress the propagation of waves and the transport mean free path of photons in random nanostructures is below than reciprocal wave vector ($k\ell_t \leq 1$) where $k = 2\pi/\lambda$ is the wave number. This regime results in photon localization in 3D, similar to Anderson localization, which was first postulated by Philip Anderson [75].

In Anderson localization, scattering induced modes with high spatial confinement. The scattered light propagates in a path that forms a closed loop with interferences occurring within it, nominating for a high degree of light confinement contributing to a standing wave pattern. This led to the finding that coherent feedback can achieve spatial resonance. Compared to the earlier discussion, the chance of scattered light returning to

its original position as a closed-loop is substantially higher in 1D and 2D structures. The localization is straightforward to achieve in a lower dimension. Anderson localization is extremely difficult to attain as scattering strength of $k\ell_t$ in a factor of 10 to 10000 (weak scattering regime) in random nanostructures. But, changes in the refractive index can cause confinements that serve as waveguides to produce resonant modes by increasing the transport mean free path value to lengthen the photon path and may result in spikes pattern as in Figure 2.5 [76]. Based upon experimental observations, both extended and localized modes can co-exist with the specifically designed random lasers.

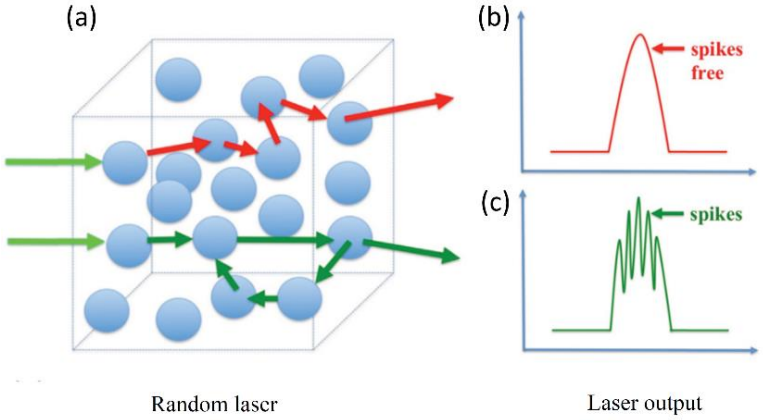

Figure 2.5: Lasing in (a) random media. Demonstrating the incoherent feedback in red arrows and coherent feedback in green arrows illustrates spectral outputs of a conventional laser and a random laser, where the (b) spikes free correspond to incoherent feedback. In contrast, the coherent feedback is recognized by its (c) spiky signature [76].

2.4 ZnO

ZnO consists of two-element, zinc and oxygen, in a solid-state at room temperature, and they exist as inorganic compound semiconductors (non-carbon-based material). ZnO owns a molar mass of 81.408 g/mol, odorless, and it is a white solid that turns yellow when heated. ZnO is an amphoteric oxide which insoluble in water but soluble in dilute alkali and acid that produce salts and water. Among the most significant zinc compounds, ZnO is the most applicable semiconductor that can be synthesized in a high-purity state and a wide range of crystal shapes and sizes [77,78].

2.4.1 Physical Properties of ZnO

ZnO is a II-IV compound semiconductor with chemical bonding, mostly covalent bonds, but for the most ion-bonded semiconductors employed in various applications, electronics, optoelectronics, and sensors . The general properties of ZnO are listed in Table 2.1 as follows;

Table 2.1: General properties of ZnO wurtzite structure [79–81].

Physical Properties	Properties
Molecular formula	ZnO
Molar mass	81.408 g/mol
Colour	Milky white solid (cold), yellow solid (heat)
Odor	Odorless
Density	5.606 g/cm^3
Melting point	1975 °C (decomposes)
Boiling point	2360 °C
Solubility in water	0.16 mg/100 mL (30 °C)
Band gap	3.37 eV (direct)
Exciton binding energy	60 meV
Sttructure	Hexagonal, $a_o=b_o\neq c_o$
Lattice parameter at 27 ºC	a_o= 3.2495 Å, b_o= 3.2495 Å, c_o= 5.2069 Å
Ideal hexagonal structure, c_o/ a_o	1.602
Refractive index (nD)	2.0041
Electron and hole effective mass	m_e*=0.28 m_o, m_h*=0.59 m_o
Lattice energy	964 kcal/mole
Dielectric constant	ε_o = 8.75, ε_∞ = 3.75
Piezoelectric coefficient	12 pC/N
Pyroelectric constant	6.8 A/s/cm^2/K x 10^{10}
Solubility	1.6 mg/L (30^{o}C)
Standard enthalpy of formation	-348.0 kJ/mol
Standard molar entropy	43.9 JK^{-1}mol^{-1}

2.4.2 Optoelectronics and Electrical Properties of ZnO

ZnO is an oxide compound semiconductor with such large bandgap energy of 3.37 eV, making it realizable in applications of high-performance electronic, optoelectronics, and photonics devices. A larger bandgap has various advantages, including less noise generation, greater breakdown voltages, the ability to withstand large electric fields (high power), and high resistance to temperature [82]. Wide bandgap energy characteristics make it an excellent semiconductor for absorbing or emitting UV light and transparency in the visible wavelength range in any application. ZnO also owns a significantly large free exciton binding energy of 60 meV that facilitates efficient excitonic emission at room temperature, and elevated temperature influenced much on the process of optical absorption and emission transition.

2.4.3 Optical Properties of ZnO

The energy band gap of ZnO is 3.37 eV, corresponding to a photon wavelength of 368 nm [83]. In terms of optical qualities, ZnO has such a high refractive index of about 2, rendering it optically transparent above the optical absorption edge of 368 nm [84], [85]. High refractive index slower light travels ($v = c/n$), causing a relatively more significant change in light direction (scattering) within the material.

2.4.4 Crystal Structure of ZnO

In theory, ZnO can be crystallized in a cubic rocksalt, zincblende, and hexagonal wurtzite as in Figure 2.6. Rendering to the first principle of the periodic research by Hartree-Fock is based on a linear combination of atomic orbitals, ZnO is thermodynamically stable and highly crystalline with the wurtzite phase, owing to its ionicity being precisely on the borderline between covalent and ionic materials. ZnO is a compound semiconductor with ionic extreme of tetragonal coordinates and hexagonal as in Figure 2.6. As a result, the bonds are classified as covalently bonded bulk materials. As reported, the electronegativity of zinc is only 1.65 to serve as an electron acceptor [86].

Nevertheless, the electronegativity of oxygen is much higher, which is 3.44, with a huge electronegativity dissimilarity; thus, ZnO is clarified as a polar covalent bond and polar semiconductor materials [87]. Therefore, ZnO preferred hexagonal wurtzite structure as the thermodynamically stable phase [87,88]. The stable wurtzite phase may be observed in normal surrounding temperature using a variety of approach parameters. The arrangement of atoms in hexagonal wurtzite structure belongs to the P63mc space group, having two lattice parameters of a_o and c_o, a_o = 3.2420 nm and c_o = 5.2098 nm, which is described by a linked lattice of Zn^{2+} and O^{2-} [89]. Figure 2.7 show ZnO structure, where each anion (O^{2-}) surrounded by four cations (Zn^{2+}), located at the corners of a approximately regular tetrahedron of sp^3 covalent bonding that structuralized along *c*-axis.

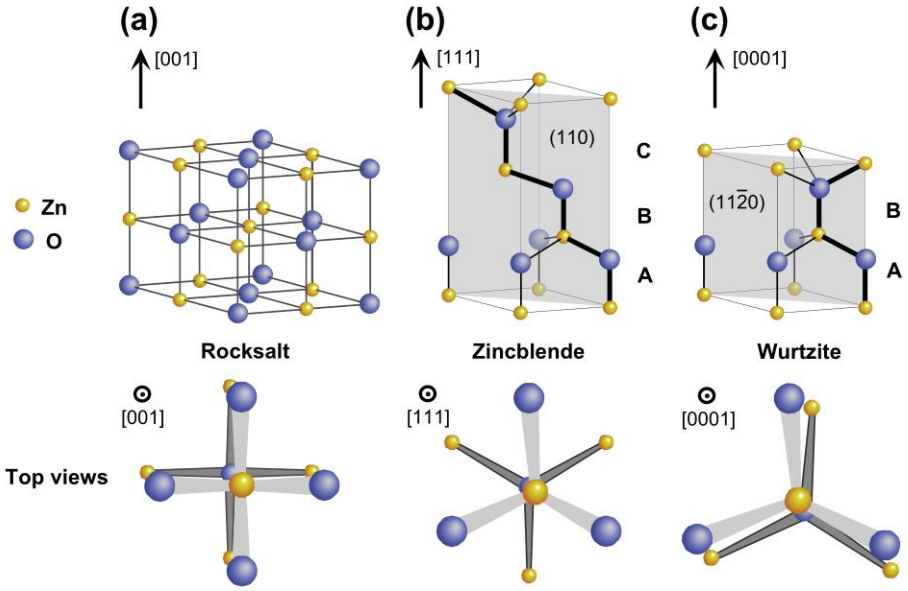

Figure 2.6: ZnO crystal structures in a stickball pattern: (a) rocksalt, (b) zincblende, and (c) hexagonal wurtzite and their Strukturbericht pattern projections plane of the (001) for rocksalt, (111) for zincblende and (0001) wurtzite, respectively [90].

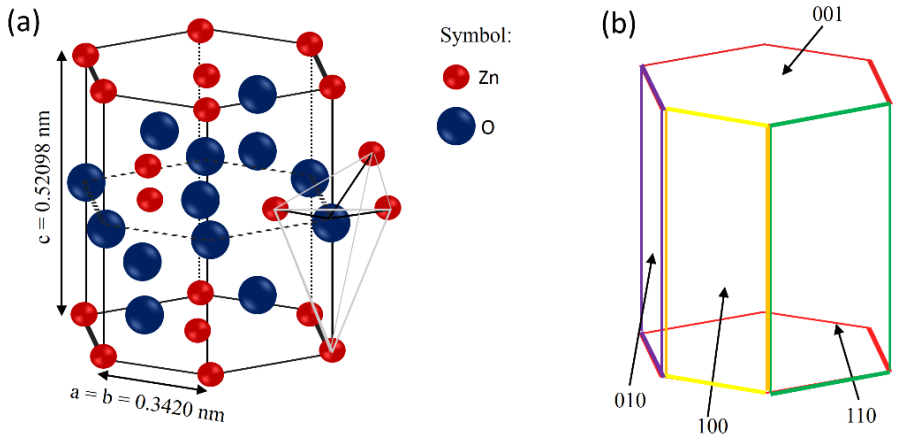

Figure 2.7: Schematic of ZnO, (a) atomic arrangement in the hexagonal wurtzite crystal structure, and (b) hexagonal crystallographic faces, polar crystal plane 001 (red lines), nonpolar crystal planes of 010 (purple lines), 100 (yellow lines), and 110 (green lines).